CHAPTER FOUR

STRUCTURAL ANALYSIS

4.1 Introduction

The determination of the structure of material (bulk or thin film) encompasses three main investigations to describe the arrangement of the building blocks of a material. These investigations are crystal structure, which deals with the shape and dimensions of the unit cell and atomic positions within it. The second investigation is the microstructure observations, which characterizes the size, shapes and orientations of the individual crystal grains. It also includes the morphology of the material surface. The third investigation is the structural defect that concerns with the defects, like point defects, dislocations and stacking faults inside the crystal grain.

The structural analysis of ZnS_xSe_{1-x} ($0 \leq x \leq 1$) thin films has been reported in the literature [4, 5, 19-25, 42-48]. These films have been prepared with different methods and under different ambient conditions. However, the variety of structures of a given material in the form of thin films can be much more than those formed in bulk because the conditions of film preparation can be varied more widely than the conditions of formation of a bulk solid. As an example, it has been found that ZnS undergoes a phase transition from cubic to hexagonal phases with larger grain size above 1020 °C [5]. Meanwhile, discrimination has been found in the preferential crystallographic orientation of polycrystalline ZnSe thin films prepared by ion-beam and electron beam depositions [21]. In this work the structure of ZnS_xSe_{1-x} thin films is

investigated using EDX, SEM and XRD techniques which have been described in chapter 2.

4.2 Results and discussion

Thickness of ZnS_xSe_{1-x} films calculated from the transmission spectrum, as discussed in chapter 3, are listed in Table 4.1 along with the deposition rate. The films were deposited by electron beam evaporation onto glass substrates at temperature ~ 60 °C. The base pressure inside the chamber was lower than 2.0×10^{-5} torr.

The individual constituents of ZnS_xSe_{1-x} thin films detected by EDX were identified from the positions of the peaks observed on the analyzer screen. Figure 4.1 shows the peaks of different elements in typical ZnS_xSe_{1-x} films examined by EDX. The main peaks were found to be corresponding to zinc (Zn), selenium (Se) and sulphur (S) from the film while the other two relatively small peaks are shown in Figure (4.1b) belong to silicon (Si) and chlorine (Cl) from the glass substrate. The peak intensities for Zn, Se and S were measured for all ZnSSe films studied in this work and recorded in counts per second (cps). The raw data of the intensities were reduced to atomic percentages using a standard ZAF computer algorithm [90] (corrections for atomic number, absorption and fluorescence). The weight percentages for the elements in the samples were calculated by normalizing the product of the atomic percentage for each element by its atomic weight. The atomic and weight percentages for Zn, Se and S are listed in Table 4.2. The theoretical stoichiometric compositional values of Zn and (S_xSe_{1-x}) in ZnS_xSe_{1-x} ($0 \leq x \leq 1$) materials are expected to be respectively, 50% and 50% in atomic percentages (AT%). The results listed in Table 4.2 show that the atomic percentage of Zn in the entire film composition is 9% less than the expected value for almost all of the samples, which means a 18% atomic percentage excess of either S, Se

Table 4.1: Film thickness and deposition rate for ZnS_xSe_{1-x} films grown by electron beam evaporation onto glass substrates at 60 °C.

Sample	Thickness nm	Deposition rate nm/Sec.	Sample	Thickness nm	Deposition rate nm/Sec.
S1	2586	10.78	S12	1632	4.53
S2	1311	3.43	S13	1740	4.83
S3	1988	5.52	S14	1742	6.45
S4	1227	3.23	S15	1760	4.89
S5	704	1.82	S16	1781	4.95
S6	2182	4.69	S17	1893	5.26
S7	828	6.90	S18	1982	5.51
S8	2015	5.60	S19	2015	5.60
S9	1668	4.63	S20	2430	9.00
S10	820	4.56	S21	1463	4.06
S11	1231	3.42	S22	232	0.60

Table 4.2: Atomic and weight percentages of Zn, Se and S, as observed in EDX, for ZnS_xSe_{1-x} samples prepared by electron beam evaporation onto glass substrates at 60 °C.

	AT%			WT%		
Sample	Zn	Se	S	Zn	Se	S
S1	43.24	51.66	5.10	39.99	57.70	2.31
S2	41.95	27.66	30.39	46.48	37.02	16.51
S3	40.84	26.66	32.50	45.9	36.18	17.91
S4	42.08	26.36	31.56	47.07	35.61	17.32
S5	40.47	23.79	35.74	46.66	33.12	20.21
S6	41.18	21.35	37.47	48.25	30.22	21.53
S7	41.10	9.07	49.83	53.73	14.32	31.95
S8	40.91	8.38	50.71	53.90	13.33	32.77
S9	40.57	7.23	52.21	54.16	11.65	34.19
S10	41.11	4.04	54.86	56.40	6.69	36.91
S11	40.52	4.09	55.39	55.78	6.81	37.41
S12	40.60	4.19	55.22	55.81	6.95	37.24
S13	40.60	4.19	55.22	55.81	6.95	37.24
S14	40.28	3.92	55.80	55.64	6.54	37.81
S15	40.60	4.19	55.22	55.81	6.95	37.24
S16	40.60	4.19	55.22	55.81	6.95	37.24
S17	40.96	4.24	54.79	56.14	7.03	36.83
S18	40.60	4.19	55.22	55.81	6.95	37.24
S19	40.52	4.09	55.39	55.78	6.81	37.41
S20	40.60	4.19	55.22	55.81	6.95	37.24
S21	40.50	1.73	57.77	57.10	2.95	39.95
S22	39.95	0.55	59.5	57.24	0.95	41.81

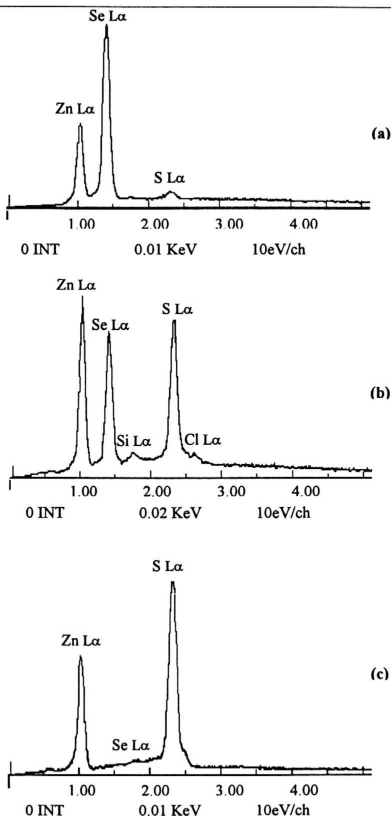

Figure 4.1: EDX profiles for ZnS_xSe_{1-x} thin films prepared by electron beam evaporation onto glass substrates at 60 °C, for samples: **(a)** S1, **(b)** S6 and **(c)** S22.

or SSe exist in the film. The results of sample S22 (in Table 4.2) show that S has almost 60% of the entire atomic composition which indicates that 20% of S (AT%) are formed as excess. However, for sample S1 (in Table 4.2) the atomic percentage of Se was almost 52% and at the same time, the atomic percentage of Zn improved to be almost 43%. Other samples have different amounts of S and Se with observed Zn (AT%) (Table 4.2) at almost 41%. In an attempt to find the relevant equations governing the deposition of ZnS_xSe_{1-x}, three deposition mechanisms may be postulated:

(I) For samples with a large amount of sulphur (i.e. S (AT%) > 50%), the excess material is expected to be S and the relevant equation will be

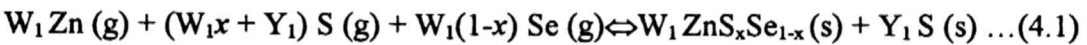

$$W_1 Zn\,(g) + (W_1x + Y_1)\,S\,(g) + W_1(1-x)\,Se\,(g) \Leftrightarrow W_1\,ZnS_xSe_{1-x}\,(s) + Y_1\,S\,(s) \quad \ldots(4.1)$$

where W_1 and Y_1 are the atomic fractions of Zn and excess S in the film, respectively. From equation 4.1 the atomic percentages for Zn, S and Se are given by

$$Zn(AT\%) = \frac{W_1}{2W_1 + Y_1} \times 100 \quad \ldots(4.2)$$

$$S(AT\%) = \frac{W_1x + Y_1}{2W_1 + Y_1} \times 100 \quad \ldots(4.3)$$

$$Se(AT\%) = \frac{W_1(1-x)}{2W_1 + Y_1} \times 100 \quad \ldots(4.4)$$

then x is given by

$$x = 1 - \frac{Se(AT\%)}{Zn(AT\%)} \quad \ldots(4.5)$$

The excess amount of S can be estimated from the relation

Excess S (AT%) =100 - 2Zn (AT%)..(4.6)

(II) For samples with a large amount of Se (i.e. Se (AT%) > 50%), the excess material is assumed to be Se and the relevant equation is expected to be

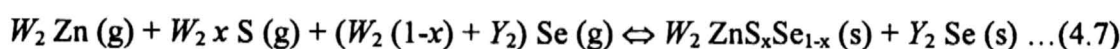

$$W_2\,Zn\,(g) + W_2\,x\,S\,(g) + (W_2\,(1\text{-}x) + Y_2)\,Se\,(g) \Leftrightarrow W_2\,ZnS_xSe_{1\text{-}x}\,(s) + Y_2\,Se\,(s) \quad ...(4.7)$$

where W_2 and Y_2 are the atomic fractions of Zn and excess Se in the sample, respectively. The value of x and the excess Se can be determined using the relations

$$x = \frac{S(AT\%)}{Zn(AT\%)} \quad ......(4.8)$$

and

Excess Se (AT%) = 100 - 2Zn (AT%)..(4.9)

(III) For samples with S (AT%) < 50% and Se (AT%) < 50%, the excess material are expected to be S, Se or SSe. If the excess material is S or Se, procedure (I) or (II) will be used respectively for the analysis, but if the excess material is SSe then the relevant equation will be

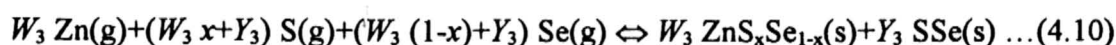

$$W_3\,Zn(g)+(W_3\,x+Y_3)\,S(g)+(W_3\,(1\text{-}x)+Y_3)\,Se(g) \Leftrightarrow W_3\,ZnS_xSe_{1\text{-}x}(s)+Y_3\,SSe(s) \quad ...(4.10)$$

where W_3 and Y_3 are the atomic fractions of Zn and excess SSe in the sample, respectively. The values of x and the excess SSe are given by

$$x = \frac{2S(AT\%) + 2Zn(AT\%) - 100}{2Zn(AT\%)} \quad \text{......(4.11)}$$

and

Excess SSe (AT%) = 100 - 2Zn (AT%)......(4.12)

Procedures (I), (II) and (III) are used to calculate x values and the excess material for ZnSSe samples under investigation. The appropriate procedure chosen for the analysis is dependent on the observed atomic percentages for S and Se in each sample. Samples S7-S22 (in Table 4.2) are analyzed following procedure (I). The results of x, excess S (AT%) and the theoretical Zn (AT%), Se (AT%) and S (AT%) (calculated from equation 4.2-4.4 by assuming $W_1 = 9$ and $Y_1 = 4$) are listed in Table 4.3. The values of W_1 and Y_1 are chosen to make the theoretical values of Zn (AT%), S (AT%) and Se (AT%) very close to the observed values. For sample S1 (in Table 4.2), the calculation is based on the mechanism described in procedure (II) and assuming $W_2 = 16$ and $Y_2 = 5$ in equation 4.7, the results are listed in Table 4.4. For samples S2-S6 (in Table 4.2) the three procedures are used separately for the analysis. The results of the calculations are displayed in Tables 4.5(a-c). The results in Table 4.5 (c) are obtained assuming $W_3 = 26$ and $Y_3 = 5$ in equation 4.10.

Figure 4.2 (a-n) shows typical scanning electron microscope photographs for ZnS_xSe_{1-x} samples grown by electron beam evaporation onto glass substrates at about 60 °C. As can be seen from the photographs, the films exhibit smooth fine-grainy surfaces with relatively large size grains embedded in a matrix of finer grains. The magnification of the photographs is not large enough to enable estimation of the grain

Table 4.3: x values and the excess S (AT%) as calculated according to procedure (I), atomic and weight percentages of Zn, Se and S according to equation 4.1 by assuming $W_1 = 9$ and $Y_1 = 4$.

Sample	X	Excess S (AT%)	Zn (AT%)	Se (AT%)	S (AT%)
S7	0.78	17.8	40.91	9.03	50.06
S8	0.80	18.18	40.91	8.38	50.71
S9	0.82	18.86	40.91	7.28	51.81
S10	0.90	17.78	40.91	4.01	55.08
S11	0.90	18.96	40.91	4.13	54.96
S12	0.90	18.8	40.91	4.21	54.88
S13	0.90	18.8	40.91	4.21	54.88
S14	0.90	19.44	40.91	3.98	55.11
S15	0.90	18.8	40.91	4.21	54.88
S16	0.90	18.8	40.91	4.21	54.88
S17	0.90	18.08	40.91	4.24	54.85
S18	0.90	18.8	40.91	4.21	54.88
S19	0.90	18.96	40.91	4.13	54.96
S20	0.90	18.8	40.91	4.21	54.88
S21	0.96	19.0	40.91	1.75	57.34
S22	0.99	20.1	40.91	0.56	58.53

Table 4.4: x values and the excess Se (AT%) as calculated according to procedure (II), atomic and weight percentages of Zn, Se and S according to equation 4.7 by assuming $W_2 = 16$ and $Y_2 = 5$.

Sample	x	Excess Se (AT%)	Zn (AT%)	Se (AT%)	S (AT%)
S1	0.12	13.52	43.24	51.66	5.10

Table 4.5 (a): x values and the excess S (AT%) as calculated according to procedure (I), atomic and weight percentages of Zn, Se and S according to equation 4.1 by assuming $W_1 = 9$ and $Y_1 = 4$.

Sample	x	Excess S (AT%)	Zn (AT%)	Se (AT%)	S (AT%)
S2	0.34	16.1	40.91	26.97	32.12
S3	0.35	18.32	40.91	26.71	32.39
S4	0.37	15.84	40.91	25.63	33.46
S5	0.41	19.06	40.91	24.05	35.04
S6	0.48	17.64	40.91	21.21	37.88

Table 4.5 (b): x values and the excess Se (AT%) as calculated according to procedure (II), atomic and weight percentages of Zn, Se and S according to equation 4.7 by assuming $W_2 = 16$ and $Y_2 = 5$.

Sample	x	Excess Se (AT%)	Zn (AT%)	Se (AT%)	S (AT%)
S2	0.72	16.1	43.24	25.43	31.33
S3	0.80	18.32	43.24	22.34	34.41
S4	0.75	15.84	43.24	24.32	32.43
S5	0.88	19.06	43.24	18.57	38.19
S6	0.91	17.64	43.24	17.41	39.35

Table 4.5 (c): x values and the excess SSe (AT%) as calculated according to procedure (III), atomic and weight percentages of Zn, Se and S according to equation 4.10 by assuming $W_3 = 26$ and $Y_3 = 5$.

Sample	x	Excess SSe (AT%)	Zn (AT%)	Se (AT%)	S (AT%)
S2	0.53	16.1	41.94	27.67	30.40
S3	0.57	18.32	41.94	26.03	32.03
S4	0.56	15.84	41.94	26.44	31.62
S5	0.65	19.06	41.94	22.84	35.22
S6	0.70	17.64	41.94	20.82	37.24

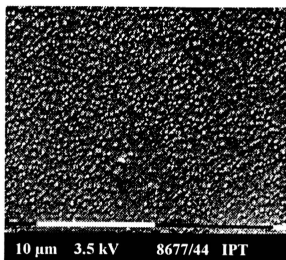

(a) S1

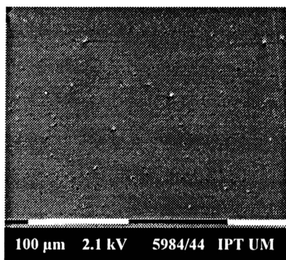

(b) S2

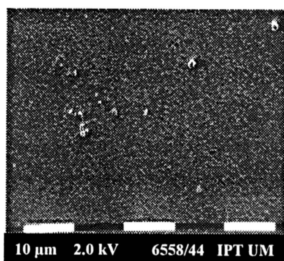

(c) S3

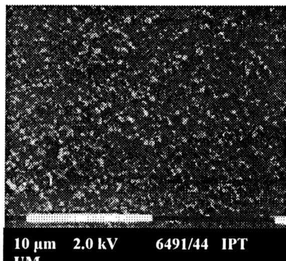

(d) S5

Figure 4.2: Scanning electron microscope photographs for polycrystalline ZnS_xSe_{1-x} thin films grown by electron beam evaporation onto glass substrates at 60 °C.

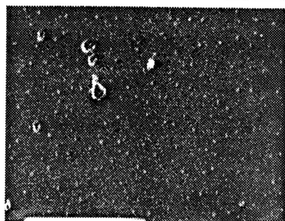

(e) S6

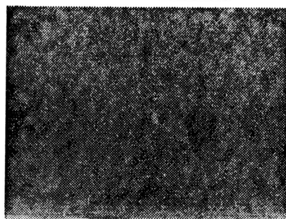

(f) S8

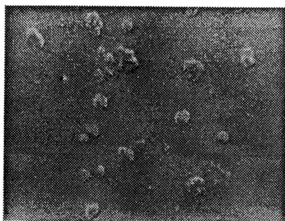

(g) S9

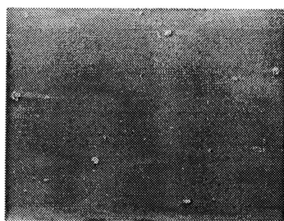

(h) S10

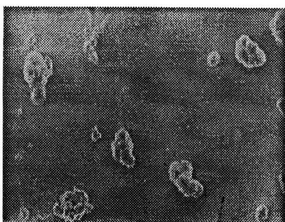

(i) S12

(j) S14

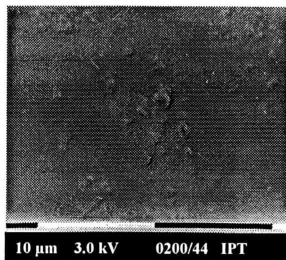

(k) S17

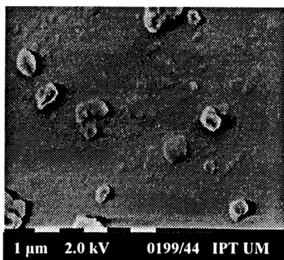

(l) S19

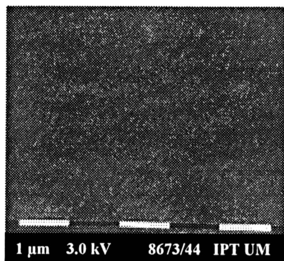

(m) S21

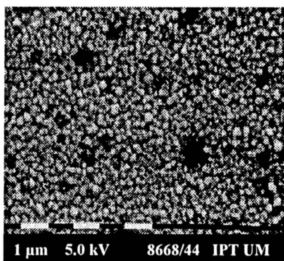

(n) S22

size on the film surface, at least 10^5 magnification is required to estimate the grain diameter which is expected to be less than 500 Å. Meanwhile, the number of the large grains is very small compared to the number of fine grains which make the estimation of the grain size for the large grains unreasonable. However, the grain size will be estimated later from the broadening of the x-ray diffraction peak.

Figure 4.3 shows typical X-ray diffraction patterns for ZnS_xSe_{1-x} samples grown by electron-beam evaporation onto glass substrates at about 60 ° C. The diffraction patterns show polycrystalline films with cubic structure. Pronounced diffraction peaks from the <111> planes have been detected. However, peaks from other planes are not detected indicating that the <111> axis is a preferential growth axis for all ZnS_xSe_{1-x} films investigated in this work. However, preferential growth of <111> axis has been observed in ZnSe films prepared by electron beam evaporation by other workers [21]. Depending on the composition of the film, the position of the <111> peak moves from $2\theta = 27.12°$ to $2\theta = 28.61°$. The inter-planar spacing d along the <111> planes has been determined from Bragg Law $\lambda = 2d\sin\theta$, where λ is the wavelength of the incident x-ray and θ is the diffraction angle. Figure 4.4 shows the variation of d with sulphur composition x in ZnS_xSe_{1-x} films. The lattice constant a_o for the cubic structure is determined from $a_o = d_{hkl}\,(h^2 + k^2 + l^2)^{1/2}$; where hkl are Miller indices for the lattice planes and d_{hkl} is the space between < hkl > lattice planes. Figure 4.5 shows the variation of a_o with x values for ZnS_xSe_{1-x} films, x values shown in Figures 4.4 and 4.5 are those computed from EDX measurements according to the three postulates assumed previously (i.e. whether the excess material is S, Se or SSe). The linear dependence of lattice constants on composition of solid solution of two compounds, to follow a line joining the values of the endpoint compounds, is known as

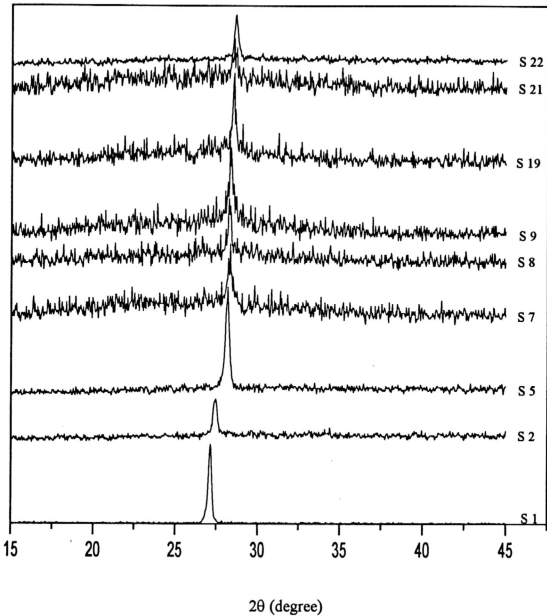

Figure 4.3: X-ray diffraction patterns for polycrystalline ZnS_xSe_{1-x} thin films grown by electron beam evaporation onto glass substrates at 60 ° C.

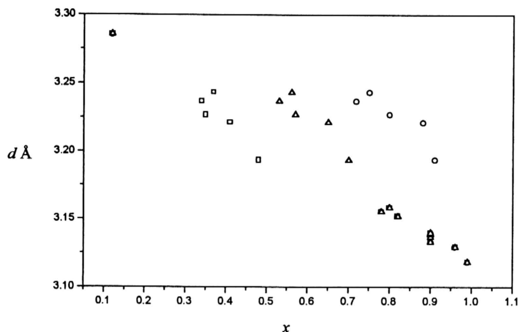

Figure 4.4: The < 111 > inter-planar spacing d versus x for ZnS_xSe_{1-x} thin films prepared by electron beam evaporation onto glass substrates at 60 ° C, x values are determined according to procedures I (□), II (○) and III (△).

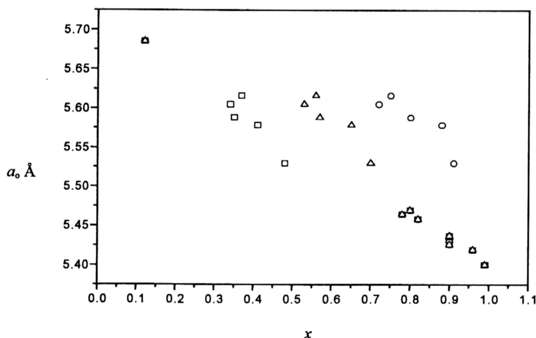

Figure 4.5: The lattice constant a_o versus x for ZnS_xSe_{1-x} thin films prepared by electron beam evaporation onto glass substrates at 60 ° C, x values are determined according to procedure I (□), II (○) and III (△).

Vegard's Law [91, 92]. The linear variation has been found in II-VI solid solution semiconductors [41, 49, 93]. However, Vegard's Law has been applied to estimate the sulphur composition x in ZnS_xSe_{1-x} thin films prepared by different techniques [42, 50]. A linear dependence of d and a_o on x is observed in Figures 4.4 and 4.5, respectively, for x values calculated according to postulate I (for the samples with S (AT%) > 50%), according to postulate II (for the samples with Se (AT%) > 50%) and according to postulate II with the assumption that the excess material is S (for the samples with S (AT%) < 50% and Se (AT%) < 50%). According to the assumptions that the excess material is Se or SSe for the samples with S (AT%) < 50% and the samples with Se (AT%)<50%, the variation of a_o with x does not follow Vegard's Law. This indicates that the first assumption; i.e. the excess material is sulphur, is more acceptable. Hereafter x values will be referred to those tabulated in Tables 4.3, 4.4 and 4.5(a) for ZnS_xSe_{1-x} films. The adoption of this assumption suggests that not all the amount of sulphur in the film is useful for the formation of ZnS_xSe_{1-x} but rather the excess amount of sulphur forms grain boundaries. X-ray diffraction patterns shown in Figure 4.3 indicate that there is no formation of polycrystalline sulphur. The excess sulphur is believed to be amorphous and forms a medium in between the grains of ZnS_xSe_{1-x}. In reference [42], it has been reported that sulphur concentration x in ZnS_xSe_{1-x} films prepared by hydrogen vapor growth could only be increased under zinc-rich conditions if the ambient conditions of ZnSe source kept unchanged. For the films studied in this work, the amount of Zn in the film is almost 41 AT% (see Table 4.2). One can expect that the amount of Se in the film controls the x value i.e. x could only be increased if the amount of Se in the film is reduced. However, if both the amounts of Se and Zn are kept unchanged in the film composition, the increase in S does not lead to an increase in x value and the excess sulphur will be formed separately as amorphous region in the

film. d and a_o values of single cubic crystals ($d = 3.123$ Å, $a_o = 5.4060$ Å for ZnS; $d = 3.273$ Å, $a_o = 5.6670$ Å for ZnSe [65]) are used as endpoints to estimate d and a_o constants for ZnS_xSe_{1-x} single crystals by assuming a linear dependence of d and a_o on x according to Vegard's Law.

Figures 4.6 and 4.7 display the estimated values of d and a_o, respectively, for ZnS_xSe_{1-x} single crystals along with the measured values for the films. It can be seen from figures 4.6 and 4.7 that both d and a_o values, for ZnS_xSe_{1-x} films, deviate from those values for single crystals. The deviation can be attributed to the existence of elastic stress inside the film lattice which in turn will be in a state of tension or compression depending on whether d and a_o values are larger or smaller than those for free-stress single crystals [92]. The existence of the elastic stress in the polycrystalline materials causes a shift to the diffraction peak position and as a result the lattice plane spacing in the constituent grains shifts from their stress-free value to some new value corresponding to the magnitude of the stress. Practically, the new lattice spacing of any particular < *hkl* > set varies from one grain to another or from one part of a grain to another. This non-uniform micro-strain causes a broadening of the corresponding diffraction peaks. The relation between the broadening produced and the non-uniformity of the strain can be obtained by differentiating the Bragg Law [92], namely

$$b = \Delta 2\theta = 2\frac{\Delta d}{d}\tan\theta \qquad (4.13)$$

where b is the broadening due to a fractional variation in plane spacing ($\Delta d/d$), where $\Delta d = d_f - d_c$; here d_f and d_c are the inter-planar spacing for stressed film and free-stress single crystal, respectively. This value of ($\Delta d/d$), however, includes both tensile and compression strains and must be divided by two to obtain the maximum broadening $B_s = b/2$ caused by tension or compression. However, in polycrystalline

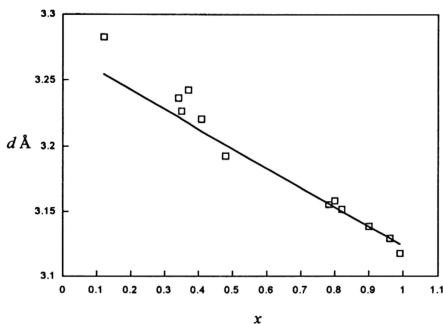

Figure 4.6: d versus x for ZnS_xSe_{1-x} single crystals (solid line) and thin films (squares) prepared by electron beam evaporation onto glass substrates at 60 ^{0} C.

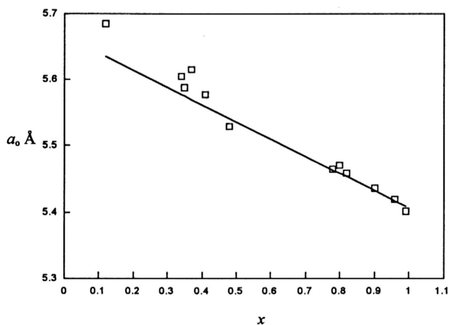

Figure 4.7: a_o versus x for ZnS_xSe_{1-x} single crystals (solid line) and thin films (squares) prepared by electron beam evaporation onto glass substrates at 60 ^{0} C.

materials with fine grains, the broadening will be due to two effects, one from the non-uniform micro-strain and the other from the fine grain size. The formula which relates the grain size to the produced broadening B_g is known as Scherrer formula and it is given by [92]

$$D = \frac{0.9\lambda}{B_g \cos\theta} \qquad (4.14)$$

where D is the diameter of the spherical grain. In this work, the measured d_f values for the polycrystalline ZnS_xSe_{1-x} films with those d_c values for ZnS_xSe_{1-x} crystals were used in equation (4.13) to calculate the broadening B_s caused by the non-uniform strain. These values of B_s were subtracted from the measured broadening B_m to estimate the broadening B_g caused by the grain size, subsequently, B_g values were used in equation (4.14) to estimate the grain diameter D. The results are tabulated in Table 4.6.

Since the crystallites that form the films under investigation exhibit a preferential growth orientation along <111> direction, a reasonable estimation of the stress magnitude can be made by considering a cubic ZnS_xSe_{1-x} crystal experiencing a tensile or compressive stress SS acts perpendicular to <111> direction. The resultant strain is defined by $\Delta a_o = (a_{of} - a_{oc})/a_{oc}$, where a_{of} and a_{oc} are the lattice constants for the ZnS_xSe_{1-x} stressed film and free-stress single crystal, respectively. The values of Δa_o for the ZnS_xSe_{1-x} films obtained in this work are within a range of $-$ 0.22% to 0.88% (see table 4.8). The ZnS_xSe_{1-x} samples with $\Delta a_o > 0$ are experiencing tension while those with $\Delta a_o < 0$ are in compression mode. Strain and stress components are related through the relation [94] given by

Table 4.6: x, 2θ, $\Delta d/d$, B_s, B_m, B_g and D values for ZnS_xSe_{1-x} thin films prepared by electron beam evaporation onto glass substrates at 60 °C.

Sample	x	2θ (degree)	$\Delta d/d$ ($\times10^{-5}$)	B_s (rad.) ($\times10^{-5}$)	B_m (rad.) ($\times10^{-5}$)	B_g (rad.) ($\times10^{-5}$)	D (Å)
S1	0.12	27.145	842	203	419	216	662
S2	0.34	27.54	441	108	349	241	593
S3	0.35	27.625	186	46	419	373	383
S4	0.37	27.485	780	191	489	298	480
S5	0.41	27.675	286	71	489	418	342
S6	0.48	27.925	-266	-66	838	904	158
S7	0.78	28.262	-30	-8	565	572	250
S8	0.8	28.236	158	40	186	147	977
S9	0.82	28.296	43	11	280	269	532
S10	0.9	28.436	-59	-15	499	511	280
S11	0.9	28.427	-28	-7	250	257	557
S12	0.9	28.414	18	5	406	401	357
S13	0.9	28.370	171	43	514	471	304
S14	0.9	28.417	6	2	673	672	213
S15	0.9	28.422	-9	-2	434	436	328
S16	0.9	28.318	351	89	173	85	1687
S17	0.9	28.441	-75	-19	339	358	400
S18	0.9	28.480	-210	-53	453	507	283
S19	0.9	28.467	-165	-42	273	315	455
S20	0.9	28.391	97	25	526	502	285
S21	0.96	28.503	-2	-0.5	638	638	224
S22	0.99	28.605	-205	-52	349	401	357

$$SS = \frac{\Delta a_o}{S_{11} + 2S_{12}} \qquad (4.15)$$

where S_{11} and S_{12} beside S_{44} are the non-zero components of the elastic compliance tensor for the cubic crystal. The relations between the elastic compliance constants (or shortly compliances) S_{ij} and the elastic stiffness constants (or shortly stiffnesses) C_{ij} are given by the following equations [94]

$$C_{11} = \frac{S_{11} + S_{12}}{(S_{11} - S_{12})(S_{11} + S_{12})} \qquad (4.16)$$

$$C_{12} = \frac{S_{12}}{(S_{11} - S_{12})(S_{11} + S_{12})} \qquad (4.17)$$

$$C_{44} = 1/S_{44} \qquad (4.18)$$

By using the stiffnesses given in Table 4.7 for ZnS [95] and ZnSe [26] single crystals, the stiffnesses and compliances (shown in table 4.8) are deduced for ZnS_xSe_{1-x} single crystals following the procedure used in reference [96]. In this procedure an elastic stiffness is defined as $C_0' = e^2/r^4$, where $e = 1.602\times10^{-19}$ C is the electronic charge and r is some characteristic length of the lattice in question. In order to apply this procedure, r is assumed to be the lattice constant a_{oc} [97], hence $C_0' = e^2/a^4_{oc}$. Using C_0' values for ZnS and ZnSe single crystals (see Table 4.7), the reduced stiffnesses C_{ij}^*, which are defined as the ordinary stiffnesses C_{ij} divided by C_o i.e. $C^*_{ij} = C_{ij} / C_0'$, are estimated (see Table 4.7). In Table 4.7, C^*_{ij} values for ZnS approximately equal to the corresponding C^*_{ij} values for ZnSe. However, C^*_{ij} are expected to be almost similar in value for II-VI compounds [96]. By averaging C^*_{ij} values of ZnS and ZnSe, C_{ij} can be estimated using C_0' values for each ZnS_xSe_{1-x} single crystal through the relation $C_{ij} = C_0' \overline{C}^*_{ij} = (e^2/a^4_{oc}) \overline{C}^*_{ij}$, where $\overline{C}^*_{ij}$ is the average value of the corresponding values of

C^{*}_{ij} for ZnS and ZnSe. The estimated C_{ij} stiffnesses and S_{ij} compliances (deduced from C_{ij} values using equations 4.16 - 4.18) for ZnS_xSe_{1-x} single crystals are listed in Table 4.8. Using equation 4.15, the stress *SS* was estimated for each ZnS_xSe_{1-x} film and the results are shown in Table 4.8. The results show that most of the films exhibit tensile stress (with positive signs), while six samples exhibit compressive stress (with negative signs). It is interesting to note that the elastic stress has been found in polycrystalline semiconductor films prepared by different techniques including sputtering [98-101]. The cause of the stress in the polycrystalline films has been studied and treated by several authors in terms of several phenomenological models [98-103]. The most appropriate model for compressive stress is the atomic peenig model, which assumes that the lattice distortion produced by energetic particles striking the condensing film causes the compressive stress [98]. On the other hand, the grain growth and grain-boundary relaxation models are used to treat the tensile stresses in evaporated films involving thermal energy particles [98]. In the model proposed by Müller [99], the theoretical and the experimental results revealed that the initial increase in tensile stress was caused by a micro-structural change from micro-columnar growth to a more densely packed atomic network with closed micro-pores.

Table 4.7: Elastic compliances S_{ij} and elastic stiffnesses C_{ij} for ZnS [95] and ZnSe [26] cubic crystals, S_{ij} values are deduced from C_{ij} values using equations (4.16-4.18), $C_0^{`}$ values and the reduced stiffnesses C_{ij}^{*} for ZnS and ZnSe single crystals.

	Compliances (10^{-13} cm^2/dyn)			Stiffnesses (10^{11} dyn/cm^2)			Lattice constant(Å)	dyn/cm^2	Reduced stiffnesses (10^{11})		
	S_{11}	S_{12}	S_{44}	C_{11}	C_{12}	C_{44}	a_{oc}	$C_0^{`}$	C^{*}_{11}	C^{*}_{12}	C^{*}_{44}
ZnS	18.52	-7.12	21.65	10.40	6.50	4.62	5.4060	3.01	3.46	2.16	1.54
ZnSe	20.67	-7.66	24.63	8.59	5.06	4.06	5.6670	2.49	3.45	2.03	1.63

Table 4.8: x and strain (Δa_o %) for ZnS_xSe_{1-x} thin films, $C_0^{`}$ values, C_{ij} and S_{ij} for ZnS_xSe_{1-x} single crystals and stress *SS* for the films.

Sample	x	Δa_o %	$C_0^{`}$ Dyn/m^2	C_{11}	C_{12}	C_{44}	S_{11}	S_{12}	S_{44}	*SS* $10^9 dyn/cm^2$
				10^{11} dyn/cm^2			10^{-13} cm^2/dyn			
S1	0.12	0.880	2.545	8.8	5.3	4.0	21	-7.9	25	17
S2	0.34	0.484	2.651	9.2	5.6	4.2	20	-7.6	24	9.8
S3	0.35	0.231	2.656	9.2	5.6	4.2	20	-7.6	24	4.7
S4	0.37	0.824	2.666	9.2	5.6	4.2	20	-7.6	24	17
S5	0.41	0.332	2.686	9.3	5.6	4.3	20	-7.5	23	6.8
S6	0.48	-0.219	2.722	9.4	5.7	4.3	20	-7.4	23	-4.6
S7	0.78	0.023	2.881	10	6.0	4.6	19	-7.0	22	0.51
S8	0.8	0.212	2.892	10	6.1	4.6	18	-7.0	22	4.7
S9	0.82	0.098	2.903	10	6.1	4.6	18	-7.0	22	2.2
S10	0.9	-0.002	2.948	10	6.2	4.7	18	-6.8	21	-0.05
S11	0.9	0.029	2.948	10	6.2	4.7	18	-6.8	21	0.64
S12	0.9	0.075	2.948	10	6.2	4.7	18	-6.8	21	1.7
S13	0.9	0.228	2.948	10	6.2	4.7	18	-6.8	21	5.1
S14	0.9	0.063	2.948	10	6.2	4.7	18	-6.8	21	1.4
S15	0.9	0.048	2.948	10	6.2	4.7	18	-6.8	21	1.1
S16	0.9	0.408	2.948	10	6.2	4.7	18	-6.8	21	9.2
S17	0.9	-0.019	2.948	10	6.2	4.7	18	-6.8	21	-0.42
S18	0.9	-0.154	2.948	10	6.2	4.7	18	-6.8	21	-3.5
S19	0.9	-0.109	2.948	10	6.2	4.7	18	-6.8	21	-2.5
S20	0.9	0.154	2.948	10	6.2	4.7	18	-6.8	21	3.5
S21	0.96	0.056	2.982	10	6.3	4.7	18	-6.8	21	1.3
S22	0.99	-0.146	3.000	10	6.3	4.8	18	-6.7	21	-3.4